UDC 539.4

Fracture Analysis of a Three-Dimensional Functionally Graded Multilayered Beam

V. I. Rizov

Department of Technical Mechanics, University of Architecture, Civil Engineering and Geodesy, Sofia, Bulgaria

V_RIZOV_FHE@uagg.bg

УДК 539.4

Аналіз руйнування тривимірної функціонально-градієнтної багатошарової балки

В. І. Різов

Факультет технічної механіки, Університет архітектури, цивільного будівництва та геодезії, Софія, Болгарія

Аналітично вивчено режим руйнування при відшаруванні для тривимірної функціонально-градієнтної багатошарової балки при визначенні зсуву на напустку з тріщиною на основі розрахунку швидкості виділення енергії деформації з використанням методів лінійно-пружної механіки руйнування. Балка може включати в себе довільну кількість шарів, кожен з яких має різні товщину і властивості компонентів. Матеріал кожного шару функціонально-градієнтний по ширині, товщині і довжині. Тріщина відшарування розташована довільно по висоті балки. Швидкість виділення енергії деформації отримано шляхом аналізу її густини у поперечному перерізі балки перед і за фронтом тріщини. Для верифікації її додатково проаналізовано за допомогою енергії деформації балки. Оцінено вплив градієнта матеріалу і розташування тріщини по висоті балки на режим руйнування при відшаруванні.

Ключові слова: функціонально-градієнтні матеріали, лінійно-пружна механіка руйнування, багатошарові конструкції.

Introduction. Since their introduction in the mid 1980s, functionally graded materials have become a promising alternative to laminated composites [1–8]. This is due to the fact that by gradual variation of material constituents composition in functionally graded materials, the interface stress concentrations are avoided, in contrast to laminated composites [9–11]. In this way, failure performances are improved. At the same time the variation of material properties in one or more spatial coordinates can be designed so as to achieve the optimum performance of members and components made of functionally graded materials to the external loads and influences. An important consideration in safety design of functionally graded materials is their fracture behavior. That is why fracture mechanics of these novel materials has received significant attention from the academic circles [12–17]. In spite of that, there are crack problems which have not been researched sufficiently. One of these problems is delamination in three-dimensional functionally graded multilayered beams.

Therefore, the main purpose of present paper was to perform an analytical study of delamination fracture in the multilayered crack lap shear (CLS) beam configuration assuming that in each layer the material is functionally graded along the width, thickness and length of layer. The fracture was studied in terms the strain energy release rate by analyzing the strain energy densities in the beam cross sections ahead and behind the crack

© V. I. RIZOV, 2018

front. The solution derived was applied to perform the parametric analysis, in order to evaluate the influences of material gradient and crack location on the delamination fracture.

1. **Delamination Analysis in Terms of the Strain Energy Release Rate**. The multilayered functionally graded CLS beam configuration analyzed in the present paper is shown schematically in Fig. 1. The beam is built up by an arbitrary number of horizontal layers. A perfect adhesion was assumed between layers. The beam cross section is a rectangle of width b and height $2h$. The beam length is l. A delamination crack of length a is located arbitrary along the beam height. The lower and upper crack arm thicknesses are h_1 and h_2, respectively. The loading consists of a horizontal force F applied at the free end of lower crack arm (Fig. 1). Thus, the upper crack arm is free of stresses. The beam is clamped in section B. The material in each layer is functionally graded along the width, thickness and length of layer.

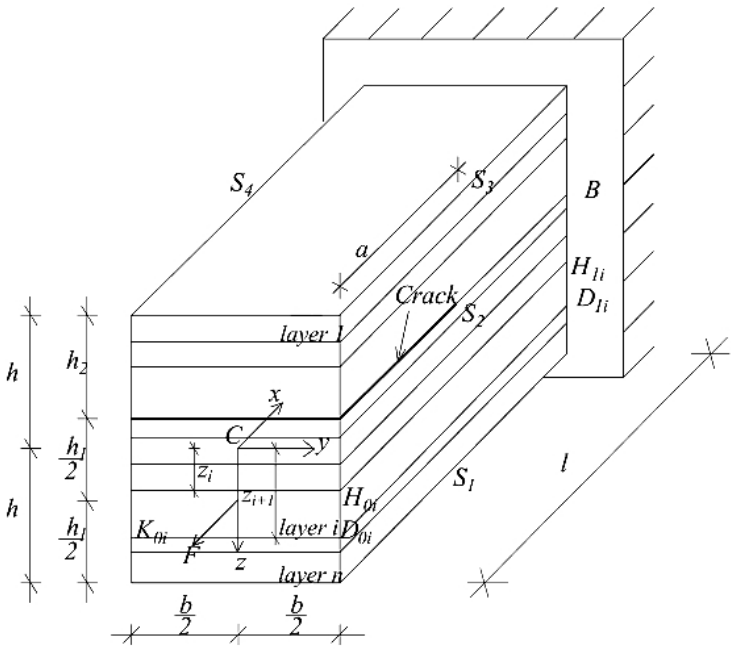

Fig. 1. Geometry and loading of the multilayered CLS beam.

The delamination fracture analysis was carried-out assuming that in each layer the modulus of elasticity E_i varies linearly along the width, thickness and length of layer. It was also assumed that in the ith layer E_{K_i}, E_{H_i}, and E_{D_i} are the values of modulus of elasticity in points K_i, H_i, and D_i, respectively, in a cross section located at distance x from the beam free end (Fig. 2). The distribution of modulus of elasticity in the ith layer was expressed in a function of y and z through E_{K_i}, E_{H_i}, and E_{D_i} by using the following equation [18] of a plane that passes via three points of coordinates $(E_{K_i}, y_{K_i}, z_{K_i})$, $(E_{H_i}, y_{H_i}, z_{H_i})$, and $(E_{D_i}, y_{D_i}, z_{D_i})$:

$$\begin{vmatrix} E_i & y & z & 1 \\ E_{K_i} & y_{K_i} & z_{K_i} & 1 \\ E_{H_i} & y_{H_i} & z_{H_i} & 1 \\ E_{D_i} & y_{D_i} & z_{D_i} & 1 \end{vmatrix} = 0, \qquad i = 1, 2, \ldots, n, \tag{1}$$

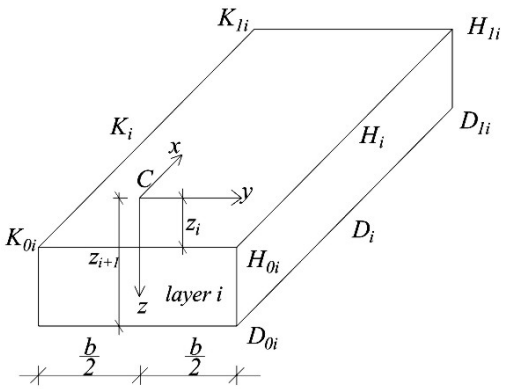

Fig. 2. Notations in the *i*th layer of CLS beam.

where (see Fig. 2)

$$y_{K_i} = -b/2, \quad z_{K_i} = z_i, \quad y_{H_i} = b/2, \quad z_{H_i} = z_i, \quad y_{D_i} = b/2, \quad z_{D_i} = z_{i+1}. \tag{2}$$

In (2), n is the number of layers.

By substituting (2) into (1), the distribution of modulus of elasticity in the *i*th layer was obtained as

$$E_i = q_{1i}\, y + q_{2i}\, z + q_{3i}, \tag{3}$$

where

$$q_{1i} = \frac{E_{K_i}(z_i - z_{i+1}) + E_{H_i}(z_{i+1} - z_i)}{b(z_{i+1} - z_i)}, \tag{4}$$

$$q_{2i} = \frac{E_{D_i} - E_{H_i}}{z_{i+1} - z_i}, \tag{5}$$

$$q_{3i} = \frac{E_{K_i}(z_{i+1} - z_i) + E_{H_i}(z_{i+1} + z_i) - 2E_{D_i} z_i}{2(z_{i+1} - z_i)}, \tag{6}$$

$$i = 1, 2, \ldots, n. \tag{7}$$

In each layer, the moduli of elasticity E_{K_i}, E_{H_i}, and E_{D_i} vary continuously along the beam length, according to the following quadratic equations:

$$E_{K_i} = E_{K_{0i}} + \frac{E_{K_{1i}} - E_{K_{0i}}}{l^2} x^2, \tag{8}$$

$$E_{H_i} = E_{H_{0i}} + \frac{E_{H_{1i}} - E_{H_{0i}}}{l^2} x^2, \tag{9}$$

$$E_{D_i} = E_{D_{0i}} + \frac{E_{D_{1i}} - E_{D_{0i}}}{l^2} x^2, \tag{10}$$

where

$$i = 1, 2, \ldots, n, \tag{11}$$

$$0 \le x \le l. \tag{12}$$

In Eqs. (8), (9), and (10), $E_{K_{0i}}$, $E_{H_{0i}}$, and $E_{D_{0i}}$ are the moduli of elasticity in points K_{0i}, H_{0i}, and D_{0i}, respectively (Fig. 2). The moduli of elasticity in points K_{1i}, H_{1i}, and D_{1i} are $E_{K_{1i}}$, $E_{H_{1i}}$, and $E_{D_{1i}}$, respectively. It can be summarized that Eqs. (3), (8), (9), and (10) describe the distribution of modulus of elasticity in the layers of functionally graded CLS beam configuration shown in Fig. 1.

The delamination was studied in terms of the strain energy release rate assuming linear-elastic behavior of the material in each layer. The strain energy release rate G can be expressed through the changes of external work ΔW_{ext} and strain energy ΔU as

$$G = \frac{\Delta W_{ext} - \Delta U}{\Delta A}, \tag{13}$$

where

$$\Delta A = b\Delta a. \tag{14}$$

In (14), Δa is a small increase of the crack length. Due to the fact that linear-elastic material behavior was assumed, the change of external work can be written as

$$\Delta W_{ext} = 2\Delta U. \tag{15}$$

The change of strain energy can be expressed as

$$\Delta U = U_b - U_a, \tag{16}$$

where U_b and U_a are the strain energies before and after the increase of crack, respectively. By substitution of (14), (15), and (16) in (13), the formula for strain energy release rate can be reduced to

$$G = \frac{U_a - U_b}{b\Delta a}. \tag{17}$$

Equation (17) was applied to calculate the strain energy release rate in the multilayered functionally graded CLS beam configuration (Fig. 1).

The strain energy before the increase of crack was derived by integrating of the strain energy density in the uncracked beam ahead of the crack front (Fig. 3)

$$U_b = \Delta a \sum_{i=1}^{i=n} \int_{z_{2i}}^{z_{2i+1}} \left(\int_{-b/2}^{b/2} u_{0ui}\, dy_2 \right) dz_2, \tag{18}$$

where z_{2i} and z_{2i+1} are the coordinates of upper and lower edges of the *i*th layer. The strain energy density u_{0ui} in the *i*th layer was written as

$$u_{0ui} = \frac{1}{2} E_i \varepsilon^2, \tag{19}$$

where E_i was determined by (3). In (19), ε is the distribution of strains.

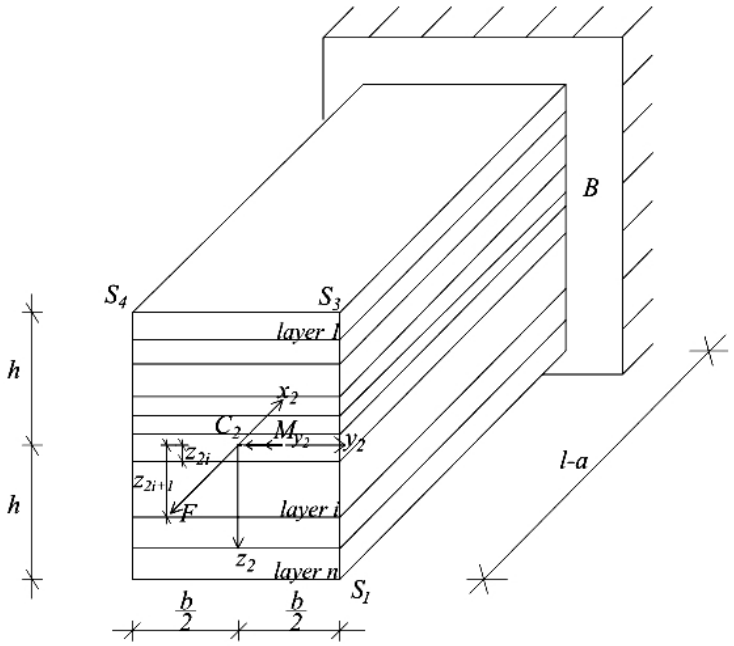

Fig. 3. The uncracked beam portion (ahead of the crack front).

An analysis of strains was carried out, in order to determine the strain energy density. The validity of the Bernoulli hypothesis for plane sections was assumed, since the span to height ratio of the beam considered is large. It should be mentioned that the Bernoulli hypothesis has been widely applied in fracture studies of functionally graded materials [15, 16]. Concerning the application of Bernoulli hypothesis in the present paper, it can also be noted that due to the fact that the multilayered functionally graded beam is loaded in eccentric tension (Fig. 1), the only non-zero strain is the longitudinal strain ε. Thus, according to the small strain compatibility equations, ε is distributed linearly in beam cross section. In the cross section $S_1S_3S_4$ ahead of the crack front (Fig. 3) the strain ε was expressed in a function of y_2 and z_2 by using the strains ε_{S_1}, ε_{S_3}, and ε_{S_4} in points S_1, S_3, and S_4. For this purpose, the following equation of a plane that passes though points $(\varepsilon_{S_4}, y_{2S_4}, z_{2S_4})$, $(\varepsilon_{S_3}, y_{2S_3}, z_{2S_3})$, and $(\varepsilon_{S_1}, y_{2S_1}, z_{2S_1})$ was applied:

$$\begin{vmatrix} \varepsilon & y_2 & z_2 & 1 \\ \varepsilon_{S_4} & y_{2S_4} & z_{2S_4} & 1 \\ \varepsilon_{S_3} & y_{2S_3} & z_{2S_3} & 1 \\ \varepsilon_{S_1} & y_{2S_1} & z_{2S_1} & 1 \end{vmatrix} = 0, \tag{20}$$

where (see Fig. 3)

$$y_{2S_4} = -b/2, \quad z_{2S_4} = -h, \quad y_{2S_3} = b/2, \quad z_{2S_3} = -h, \quad y_{2S_1} = b/2, \quad z_{2S_1} = h. \tag{21}$$

By substituting (21) into (20), we get

$$\varepsilon = r_1 y_2 + r_2 z_2 + r_3, \tag{22}$$

where

$$r_1 = \frac{1}{b}(\varepsilon_{S_3} - \varepsilon_{S_4}), \tag{23}$$

$$r_2 = \frac{1}{2h}(\varepsilon_{S_1} - \varepsilon_{S_3}), \tag{24}$$

$$r_3 = \frac{1}{2}(\varepsilon_{S_1} + \varepsilon_{S_4}). \tag{25}$$

The quantities r_1, r_2, and r_3 were determined from the following equations for equilibrium of the beam cross section ahead of the crack tip:

$$N = \sum_{i=1}^{i=n} \int_{z_{2i}}^{z_{2i+1}} \left(\int_{-b/2}^{b/2} \sigma_i \, dy_2 \right) dz_2, \tag{26}$$

$$M_{y_2} = \sum_{i=1}^{i=n} \int_{z_{2i}}^{z_{2i+1}} \left(\int_{-b/2}^{b/2} \sigma_i \, z_2 dy_2 \right) dz_2, \tag{27}$$

$$M_{z_2} = \sum_{i=1}^{i=n} \int_{z_{2i}}^{z_{2i+1}} \left(\int_{-b/2}^{b/2} \sigma_i \, y_2 dy_2 \right) dz_2, \tag{28}$$

where N, M_{y_2}, and M_{z_2} are the axial force and the bending moments for the y_2- and z_2-axis, respectively (Fig. 3). It is obvious that (Figs. 1 and 3)

$$N = F, \qquad M_{y_2} = F\left(h - \frac{h_1}{2}\right), \qquad \text{and} \qquad M_{z_2} = 0. \tag{29}$$

The stress distribution σ_i in the ith layer was calculated by the Hooke law

$$\sigma_i = E_i \varepsilon. \tag{30}$$

In order to perform the integration in (26), (27), and (28), the modulus of elasticity (3) was transformed as (Fig. 3)

$$E_i = q_{1i} y_2 + q_{2i} z_2 + q_{3i}. \tag{31}$$

By substituting of (30) and (31) in (26), (27), and (28), we derived

$$N = \sum_{i=1}^{i=n} \left[q_{1i} r_1 \frac{b^3}{12}(z_{2i+1} - z_{2i}) + q_{2i} r_2 \frac{b}{3}(z_{2i+1}^3 - z_{2i}^3) + q_{3i} r_2 \frac{b}{2}(z_{2i+1}^2 - z_{2i}^2) + \right.$$

$$\left. + q_{2i} r_3 \frac{b}{2}(z_{2i+1}^2 - z_{2i}^2) + q_{3i} r_3 b(z_{2i+1} - z_{2i+1}) \right], \tag{32}$$

$$M_{y_2} = \sum_{i=1}^{i=n}\left[q_{1i}r_1\frac{b^3}{24}(z_{2i+1}^2 - z_{2i}^2) + q_{2i}r_2\frac{b}{4}(z_{2i+1}^4 - z_{2i}^4) + \right.$$

$$\left. + q_{3i}r_2\frac{b}{3}(z_{2i+1}^3 - z_{2i}^3) + q_{2i}r_3\frac{b}{3}(z_{2i+1}^3 - z_{2i}^3) + q_{3i}r_3\frac{b}{2}(z_{2i+1}^2 - z_{2i}^2)\right], \tag{33}$$

$$M_{z_2} = \sum_{i=1}^{i=n}\left[q_{2i}r_1\frac{b^3}{24}(z_{2i+1}^2 - z_{2i}^2) + q_{3i}r_1\frac{b^3}{12}(z_{2i+1} - z_{2i}) + \right.$$

$$\left. + q_{1i}r_2\frac{b^3}{24}(z_{2i+1}^2 - z_{2i}^2) + q_{1i}r_3\frac{b^3}{12}(z_{2i+1} - z_{2i})\right]. \tag{34}$$

Equations (32), (33), and (34) should be solved with respect to r_1, r_2, and r_3 by using the MatLab computer program. Then the strain distribution in the beam cross section ahead of the crack front can be obtained by substituting of r_1, r_2, and r_3 in (31).

It should be noted that at $E_{K_i} = E_{H_i} = E_{D_i} = E$ from (22), (32), (33), and (34), we get

$$\varepsilon = \frac{F}{2bhE} + \frac{3F\left(h - \dfrac{h_1}{2}\right)}{2bh^3E}z_2, \tag{35}$$

which exacted matches the formula for strain distribution [19] in a homogeneous beam of rectangular cross section $b \times 2h$ loaded by the eccentric tension by a force F at eccentricity $h - h_1/2$.

The strain energy after the increase of crack U_a was obtained by integration of the strain energy density in the lower crack arm only (the upper crack arm is free of stresses)

$$U_a = \Delta a \sum_{i=1}^{i=n_L}\int_{z_{1i}}^{z_{1i+1}}\left(\int_{-b/2}^{b/2} u_{0li}\,dy_1\right)dz_1, \tag{36}$$

where z_{1i} and z_{1i+1} are the coordinates of upper and lower edges of the *i*th layer (Fig. 4), n_L is the number of layers in the lower crack arm, u_{0li} is the strain energy density in the *i*th layer which was written as

$$u_{0li} = \frac{1}{2}E_i\varepsilon^2. \tag{37}$$

In (37), E_i and ε are the distributions of modulus of elasticity and strains, respectively.

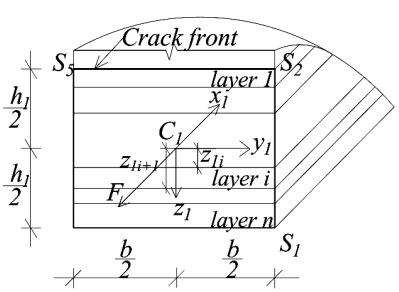

Fig. 4. The lower crack arm cross section behind the crack front.

Equation (3) was used to describe the distribution of modulus of elasticity in the lower crack arm cross section. For this purpose, (3) was re-written as

$$E_i = q_{1i}\, y_1 + q_{2i}\, z_1 + q_{3i}\,, \tag{38}$$

where the axes y_1 and z_1 are shown in Fig. 4.

In order to express the distribution of strains, Eq. (22) was reduced to

$$\varepsilon = r_{1l}\, y_1 + r_{2l}\, z_1 + r_{3l}\,, \tag{39}$$

where the quantities r_{1l}, r_{2l}, and r_{3l} were determined from Eqs. (32), (33), and (34). For this purpose, n, r_1, r_2, r_3, z_{2i}, and z_{2i+1} were replaced with n_L, r_{1l}, r_{2l}, r_{3l}, z_{1i}, and z_{1i+1}, respectively. Besides, $M_{y_2} = 0$ was substituted in (29).

Finally, by substituting of (18), (19), (22), (30), (31), (36), (37), (38), and (39) in (17), we derived

$$\begin{aligned} G = \sum_{i=1}^{i=n_L} \Bigg[& r_{1l} r_{2l} q_{1i} \frac{b^2}{24} (z_{1i+1}^2 - z_{1i}^2) + r_{1l} r_{3l} q_{1i} \frac{b^2}{12} (z_{1i+1} - z_{1i}) + r_{1l}^2 q_{2i} \frac{b^2}{48} (z_{1i+1}^2 - z_{1i}^2) + \\ & + \frac{1}{8} r_{2l}^2 q_{2i} (z_{1i+1}^4 - z_{1i}^4) + \frac{1}{4} r_{3l}^2 q_{2i} (z_{1i+1}^2 - z_{1i}^2) + \frac{1}{3} r_{1l} r_{3l} q_{2i} (z_{1i+1}^3 - z_{1i}^3) + \\ & + r_{1l}^2 q_{3i} \frac{b^2}{24} (z_{1i+1} - z_{1i}) + \frac{1}{6} r_{2l}^2 q_{3i} (z_{1i+1}^3 - z_{1i}^3) + \frac{1}{2} r_{3l}^2 q_{3i} (z_{1i+1} - z_{1i}) + \\ & + \frac{1}{2} r_{1l} r_{3l} q_{3i} (z_{1i+1}^2 - z_{1i}^2) \Bigg] - \\ & - \sum_{i=1}^{i=n} \Bigg[r_1 r_2 q_{1i} \frac{b^2}{24} (z_{2i+1}^2 - z_{2i}^2) + r_1 r_3 q_{1i} \frac{b^2}{12} (z_{2i+1} - z_{2i}) + \\ & + r_1^2 q_{2i} \frac{b^2}{48} (z_{2i+1}^2 - z_{2i}^2) + \frac{1}{8} r_2^2 q_{2i} (z_{2i+1}^4 - z_{2i}^4) + \frac{1}{4} r_3^2 q_{2i} (z_{2i+1}^2 - z_{2i}^2) + \\ & + \frac{1}{3} r_1 r_3 q_{2i} (z_{2i+1}^3 - z_{2i}^3) + r_1^2 q_{3i} \frac{b^2}{24} (z_{2i+1} - z_{2i}) + \frac{1}{6} r_2^2 q_{3i} (z_{2i+1}^3 - z_{2i}^3) + \\ & + \frac{1}{2} r_3^2 q_{3i} (z_{2i+1} z_{2i}) + r_1 r_{3l} q_{3i} (z_{2i+1}^2 - z_{2i}^2) \Bigg]. \end{aligned} \tag{40}$$

Equation (40) calculates the strain energy release rate in the multilayered functionally graded CLS beam configuration.

At $E_{K_i} = E_{H_i} = E_{D_i} = E$ and $h_1 = h$, Eq. (40) transforms in

$$G = \frac{F^2}{16 E b^2 h}, \tag{41}$$

which coincides with the expression for strain energy release rate in homogeneous CLS when the crack is in the beam mid-plane [20].

In order to verify (40), an additional analysis of the strain energy release rate was developed by using the fact that for linear-elastic materials the strain energy release rate can be written as

$$G = \frac{dU}{dA}, \tag{42}$$

where U is the beam strain energy. In view of the fact that

$$dA = bda, \tag{43}$$

Eq. (42) was re-written as

$$G = \frac{dU}{bda}. \tag{44}$$

Since the upper crack arm is stress-free, the beam strain energy was calculated by integrating the strain energy density in the lower crack arm and in the uncracked beam portion

$$U = \sum_{i=1}^{i=n_L} \int_{z_{1i}}^{z_{1i+1}} \left[\int_{-b/2}^{b/2} \left(\int_{0}^{a} u_{0li}\, dx \right) dy_1 \right] dz_1 + \sum_{i=1}^{i=n} \int_{z_{2i}}^{z_{2i+1}} \left[\int_{-b/2}^{b/2} \left(\int_{a}^{l} u_{0ui}\, dx \right) dy_2 \right] dz_2. \tag{45}$$

By substituting of (19), (30), (31), (37), (38), (39), and (45) in (44), we obtained expression for the strain energy release rate that matches exactly (40). This fact verifies the fracture analysis developed in the present paper.

The effects of material gradient and crack location along the beam height on the delamination fracture behavior were evaluated. For this purpose, calculations of the strain energy release rate were performed by using Eq. (40). The results obtained were presented in nondimensional form by using the formula $G_N = G \Big/ (E_{D_{01}} b)$. Two three-layered CLS beam configurations were considered (Fig. 5).

In the first configuration, the delamination crack is located between layers *2* and *3* (Fig. 5a). In the configuration in Fig. 5b the delamination is between layers *1* and *2*. It was assumed that $t_l = 0.0025$ m, $b = 0.025$ m, and $F = 70$ N.

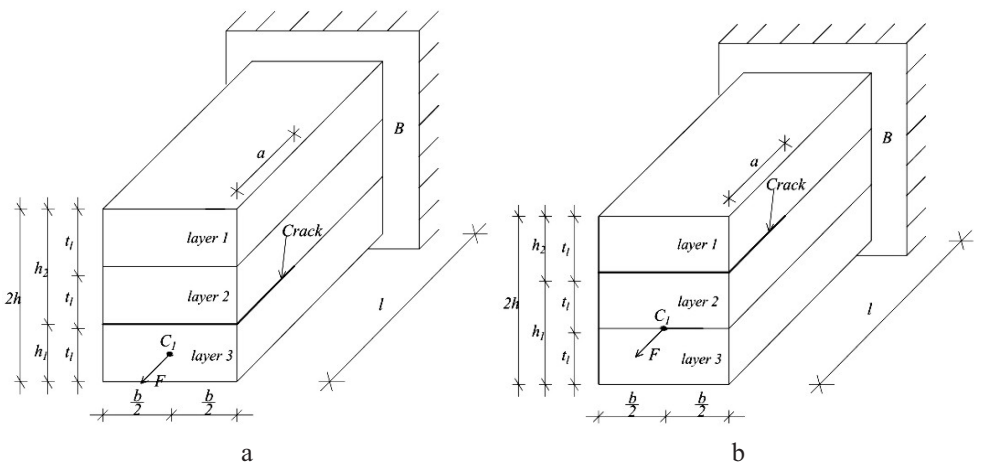

Fig. 5. Two three-layered CLS beam configurations.

The material gradient along the vertical edge $H_{03}D_{03}$ of layer *3* was characterized by $E_{H_{03}}/E_{D_{03}}$ ratio. It should be mentioned that $E_{D_{03}}$ was kept constant in the calculations. Thus, $E_{H_{03}}$ was varied in order to generate various $E_{H_{03}}/E_{D_{03}}$ ratios. The strain energy release rate in nondimensional form was plotted against $E_{H_{03}}/E_{D_{03}}$ ratio for the two three-layered CLS beam configurations at $a/l = 0.5$, $E_{D_{03}}/E_{D_{01}} = 1.5$, $E_{K_{03}}/E_{D_{03}} = 0.5$, $E_{D_{13}}/E_{D_{03}} = 2$, $E_{H_{13}}/E_{H_{03}} = 2$, $E_{K_{13}}/E_{K_{03}} = 2$, $E_{H_{01}}/E_{D_{01}} = 1$, $E_{K_{01}}/E_{D_{01}} = 2$, $E_{D_{11}}/E_{D_{01}} = 0.5$, $E_{H_{11}}/E_{H_{01}} = 0.5$, $E_{K_{11}}/E_{K_{01}} = 0.5$, $E_{D_{02}}/E_{D_{01}} = 1$, $E_{H_{02}}/E_{D_{02}} = 0.5$, $E_{K_{02}}/E_{D_{02}} = 1$, $E_{D_{12}}/E_{D_{02}} = 1$, $E_{H_{12}}/E_{H_{02}} = 1$, and $E_{K_{12}}/E_{K_{02}} = 1$ in Fig. 6. The curves in Fig. 6 indicate that the strain energy release rate decreases with increasing of $E_{H_{03}}/E_{D_{03}}$ ratio. This finding was attributed to the increase of beam stiffness. One can observe in Fig. 6 that the strain energy release rate is higher when the crack is located between layers *2* and *3* in comparison with the case when the crack is between layers *1* and *2*. This is due to the increase of lower crack arm stiffness (the upper crack arm is free of stresses) and to the decrease of eccentricity of force F in the uncracked beam portion ahead of the crack front when the crack is between layers *1* and *2*.

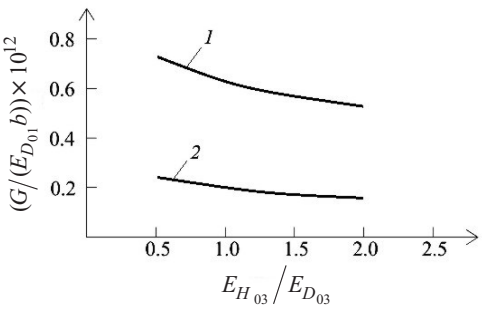

Fig. 6

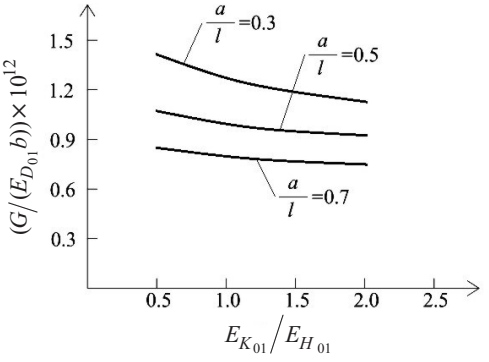

Fig. 7

Fig. 6. The strain energy release rate in nondimensional form plotted against $E_{H_{03}}/E_{D_{03}}$ ratio: (*1*), (*2*) for the beam configuration in Fig. 5a and Fig. 5b, respectively.

Fig. 7. The strain energy release rate in nondimensional form presented as a function of $E_{K_{01}}/E_{H_{01}}$ ratio at three a/l ratios.

The effect of crack length was analyzed too. The crack length was characterized by a/l ratio. Calculations of the strain energy release rate were performed for the crack in Fig. 5a. The strain energy release rate in nondimensional form was presented as function of $E_{K_{01}}/E_{H_{01}}$ ratio for three a/l ratios at $E_{H_{01}}/E_{D_{01}} = 1$, $E_{D_{11}}/E_{D_{01}} = 2$, $E_{H_{11}}/E_{H_{01}} = 2$, $E_{K_{11}}/E_{K_{01}} = 2$, $E_{D_{02}}/E_{D_{01}} = 1$, $E_{H_{02}}/E_{D_{02}} = 0.5$, $E_{K_{02}}/E_{D_{02}} = 2$, $E_{D_{12}}/E_{D_{02}} = 2$, $E_{H_{12}}/E_{H_{02}} = 2$, $E_{K_{12}}/E_{K_{02}} = 2$, $E_{H_{03}}/E_{D_{03}} = 0.5$, $E_{D_{03}}/E_{D_{01}} = 1.5$, $E_{K_{03}}/E_{D_{03}} = 0.5$, $E_{D_{13}}/E_{D_{03}} = 2$, $E_{H_{13}}/E_{H_{03}} = 2$, and $E_{K_{13}}/E_{K_{03}} = 2$ in Fig. 7. It can be observed in Fig. 7 that the strain energy release rate decreases with increasing of a/l ratio (this can be explained with the increase of modulus of elasticity in the beam cross section, in which

the crack front is located, since the modulus of elasticity in the clamped end of beam is higher than in the free end of beam). Besides, the strain energy release rate decreases with $E_{K_{01}} \big/ E_{H_{01}}$ ratio (Fig. 7).

Conclusions. An analytical study of the delamination fracture in the functionally graded multilayered CLS beam configuration was carried out. A perfect adhesion was assumed between layers. The beam can have any number of layers. Besides, each layer can have different thickness and material properties. Also, in each layer the material is functionally graded along the width, thickness and length of layer. The delamination crack can be located arbitrary along the beam height. It was assumed that in each layer the modulus of elasticity varies linearly along the width and thickness of layer. Along the layer length, the modulus of elasticity varies in a quadratic law. The fracture was studied in terms of the strain energy release rate assuming linear-elastic material behavior. A closed form analytical solution for the strain energy release rate was derived by analysing the strain energy densities in the beam cross sections ahead and behind the crack front. In order to verify the solution, an additional analysis of the strain energy release rate was performed by using the beam strain energy. The influence of material gradient and crack location along the beam height on the delamination fracture behavior was analyzed. It was found that the strain energy release rate decreases with $E_{H_{03}} \big/ E_{D_{03}}$ and $E_{K_{01}} \big/ E_{H_{01}}$ ratios. The analysis revealed also that the strain energy release rate decreases with crack length when the modulus of elasticity in the clamped end of beam is higher than in the free one. The analytical solution derived in the present paper is useful for parametric studies since the simple formulas obtained capture the essentials of delamination fracture behavior of the three-dimensional functionally graded multilayered SCL beam.

Acknowledgments. The present study was supported financially by the Research and Design Centre (CNIP) of the UACEG, Sofia (Contract BN – 189/2016).

Р е з ю м е

Аналитически изучен режим разрушения при отслоении для трехмерной функционально-градиентной многослойной балки для определения сдвига на нахлестке с трещиной на основе расчета скорости выделения энергии деформации с использованием методов линейно-упругой механики разрушения. Рассматриваемая конфигурация балки может состоять из произвольного количества слоев, имеющих различные толщину и свойства компонентов. Материал каждого слоя функционально градиентен по ширине, толщине и длине. Трещина отслоения расположена произвольно по высоте балки. Скорость выделения энергии деформации получена путем анализа ее плотности в поперечном сечении балки перед и за фронтом трещины. Для верификации она дополнительно проанализирована с помощью энергии деформации балки. Выполнена оценка влияния градиента материала и расположения трещины по высоте балки на режим разрушения при отслоении.

1. M. Koizumi, “The concept of FGM,” *Ceram. Trans. Funct. Grad. Mater.*, **34**, 3–10 (1993).
2. A. Mortensen and S. Suresh, “Functionally graded metals and metal-ceramic composites: Part 1 Processing,” *Int. Mater. Rev.*, **40**, No. 6, 239–265 (1995).
3. A. Neubrand and J. Rödel, “Gradient materials: An overview of a novel concept,” *Z. Metallkd.*, **88**, 358–371 (1997).
4. S. Suresh and A. Mortensen, *Fundamentals of Functionally Graded Materials*, IOM Communications Ltd, London (1998).

5. T. Hirai and L. Chen, "Recent and prospective development of functionally graded materials in Japan," *Mater Sci. Forum*, **308–311**, 509–514 (1999).
6. M. M. Gasik, "Functionally graded materials: bulk processing techniques," *Int. J. Mater. Prod. Tec.*, **39**, 20–29 (2010).
7. M. M. Nemat-Allal, M. H. Ata, M. R. Bayoumi, and W. Khair-Eldeen, "Powder metallurgical fabrication and microstructural investigations of aluminum/steel functionally graded material," *Mater. Sci. Appl.*, **2**, 1708–1718 (2011).
8. S. K. Bohidar, R. Sharma, and P. R. Mishra, "Functionally graded materials: A critical review," *Int. J. Res.*, **1**, 289–301 (2014).
9. A. Szekrényes, "Delamination fracture analysis in the G_{II}–G_{III} plane using prestressed composite beams," *Int. J. Solids Struct.*, **44**, 3359–3378 (2007).
10. A. Szekrényes, "The influence of crack length and delamination width on the mode-III energy release rate of laminated composites," *J. Compos. Mater.*, **45**, No. 3, 279–294 (2011).
11. A. Szekrényes, "Semi-layerwise analysis of laminated plates with nonsingular delamination – The theorem of autocontinuity," *Appl. Math. Model*., **40**, No. 2, 1344–1371 (2016).
12. F. Erdogan, "Fracture mechanics of functionally graded materials," *Compos. Eng*., **5**, No. 7, 753–770 (1995).
13. G. H. Paulino, "Fracture of functionally graded materials," *Eng. Fract. Mech.*, **69**, Nos. 14–16, 1519–1520 (2002).
14. M. T. Tilbrook, R. J. Moon, and M. Hoffman, "Crack propagation in graded composites," *Compos. Sci. Technol.*, **65**, No. 2, 201–220 (2005).
15. A. Carpinteri and N. Pugno, "Cracks in re-entrant corners in functionally graded materials," *Eng. Fract. Mech.*, **73**, No. 10, 1279–1291 (2006).
16. A. K. Upadhyay and K. R. Y. Simha, "Equivalent homogeneous variable depth beams for cracked FGM beams; compliance approach," *Int. J. Fracture*, **144**, 209–213 (2007).
17. S.-D. Pan, J.-C. Feng, Z.-G. Zhou, and L.-Z. Wu, "Four parallel non-symmetric mode-III cracks with different lengths in a functionally graded material plane," *Strength Fract. Compl.*, **5**, Nos. 3–4, 143–166 (2009).
18. G. A. Korn and T. M. Korn, *Mathematical Handbook for Scientists and Engineers*, McGraw-Hill, New York (1961).
19. N. E. Dowling, *Mechanical Behavior of Materials*, Pearson (2007).
20. J. W. Hutchinson and Z. Suo, "Mixed mode cracking in layered materials," *Adv. Appl. Mech.*, **29**, 63–191 (1991).

Received 15. 12. 2016